AIMS Materials Science, 11(2): 295–308.
DOI: 10.3934/matersci.2024016
Received: 07 December 2023
Revised: 05 February 2024
Accepted: 19 February 2024
Published: 15 March 2024

http://www.aimspress.com/journal/Materials

Research article

Electrolyte-plasma surface hardening of hollow steel applicator needles for point injection of liquid mineral fertilizers

Bauyrzhan Rakhadilov[1], Moldir Bayandinova[1], Rinat Kussainov[2] and Almasbek Maulit[1,2,*]

[1] PlasmaScience LLP, Ust-Kamenogorsk 070000, Kazakhstan
[2] The Engineering-Technological Faculty, Shakarim University, Semey 071412, Kazakhstan

* **Correspondence:** Email: maulit.almas@gmail.com; Tel.: +7-771-355-3211.

Abstract: This paper presents the results of research on the effect of electrolyte-plasma hardening on tribological and mechanical properties of hollow needles of 12Kh18N10T steel applicators for liquid fertilizer application. For the application of liquid fertilizers for processing and testing, the hollow needles of the applicator are made of 12Kh18N10T steel of cylindrical shape with a diameter of 20 mm. To ensure uniformity of the hardening process, the part was rotated clockwise during the entire procedural cycle. To reveal the influence of the sample rotation speed on the uniform surface hardening, an experiment was conducted for three applicators with rotation speeds of 4, 6, and 8 rev/min. As a result of electrolyte-plasma surface hardening (EPSH), the phase composition of the specimen's surface is characterized by the presence of austenite (γ-Fe) and ferrite (α-Fe). It is revealed that the maximum value of microhardness after EPSH is 2 times higher than the initial value. According to the results of the performed works, the contract on application of tests in field conditions and revealing of perspectivity of needle applicators for liquid fertilizers application was concluded.

Keywords: electrolyte-plasma hardening; steel 12Kh18N10T; applicator; wear resistance; hardness

1. Introduction

Protection of agricultural machinery from corrosion and wear is an important and complex task, requiring large expenditures of material resources both in the manufacture of machines and the period of their operation, storage, and repair [1,2]. Machines for mineral fertilizer application are the most

subject to corrosion and wear [3]. This is explained by specific working conditions in which machine parts are in contact with mineral fertilizers and abrasive soil particles that cause corrosion and wear of metal.

Today the market of agricultural machinery offers a sufficient number of various machines for mineral fertilizer application. Among them, the most promising are the systems for liquid mineral fertilizer application using rotary point injectors, which place fertilizer more optimally [4–7]. These systems use spikes attached to a rotating wheel to inject liquid fertilizer into the soil at precise intervals and depths with minimal root damage and soil disturbance. Root zone fertilizer application systems improve nutrient use efficiency and increase crop yields [8].

One of the problems preventing the widespread use of units for spot application of liquid fertilizers into the soil is the frequent replacement of needle (nozzle) wheels on this device due to the destruction of its working surface from corrosive wear. Usually, the needle wheels of the unit for spot application of liquid fertilizers are made of stainless steel, titanium alloy, and stainless steel with tungsten carbide tips [9–11]. Needle wheels made of stainless steel with tungsten carbide tips and titanium alloy will be relatively long lasting. However, they are expensive. Because of the relatively low cost of stainless-steel needles, domestic agricultural enterprises widely use needles made of 12Kh18N10T stainless steel [12]. However, 12Kh18H10T stainless steel is highly susceptible to wear due to the influence of aggressive composition of fertilizers and abrasive soil particles.

Resisting wear on parts mainly requires surface treatment. Today, electrolyte plasma surface hardening (EPSH) can be considered one of the most promising and relevant surface treatment technologies. This method has been proven to improve the desired physical and mechanical properties in a much shorter time (a few seconds) compared to traditional heat treatment processes, which can take from several hours to several days [13].

In our previous works [14,15], a comparative study of the effect of volumetric and surface heat treatment on the structural phase state of medium carbon steels was carried out. Surface hardening was carried out by the electrolyte plasma method. Bulk quenching was carried out by heating to 900 °C followed by cooling in water and oil, and some quenched samples were annealed at 510 °C. The results showed that surface quenching by electrolytic plasma increased the microhardness by two times due to the formation of fine-needle martensite. This proves that the electrolyte plasma quenching method can be considered as an alternative to the conventional furnace heating and cooling method.

The authors in [16] presented the results of electrolytic plasma heat treatment of AISI1040 steel. The results show that the hardness of AISI1040 steel is about 250 HV0.2 and the hardness after surface heat treatment is about 1000–1050 HV0.2. The treated samples show better wear resistance. The overlapped zone is a tempering zone and consists of sorbitite and tempered martensite. The hardness of sorbitite is much lower than that of martensite. Thus, the wear resistance of AISI1040 samples is reduced. Based on this, the results obtained by these authors also confirm that EPSH improves the physical and mechanical properties and positively affects the service life under service conditions [17–19].

In order to improve mechanical properties, it is recommended to develop an EPSH regime based on the application of cyclic thermal effects. The obtained hardening structures have high hardness, wear resistance, and crack resistance. Therefore, we studied the influence of electrolyte-plasma hardening on tribological and mechanical properties of hollow needles of 12Kh18N10T steel applicator for liquid fertilizer application.

2. Materials and methods

As a material of the study for electrolyte-plasma surface hardening (EPSH), 4 samples from 12Kh18N10T steel were taken. EPSH of steel was carried out in the cathodic regime at the electrolyte-plasma treatment unit [20,21]. The power source was a powerful rectifier giving a maximum output value of 360 V/100 A in the form of direct current [22,23]. A sodium carbonate (Na_2CO_3) solution was used as the heating and cooling source. The composition of the electrolyte is 80 wt.% distilled water and 20 wt.% Na_2CO_3. The voltage value (V) and treatment time (s) were different for each specimen. The samples were hardened at voltages of 320, 300 V, in sequence. To determine the optimal quenching regimen, a series of experiments were conducted. Each of the four samples utilized a homogeneous electrolyte composition. Parameters such as voltage, quenching duration, and cooling were varied. The sample processing modes are shown in Table 1.

The first sample underwent quenching for 2 s at a voltage of 320 V, followed by cooling with electrolyte to room temperature. The second sample underwent cyclic treatment: initial quenching for 2 s at 320 V, followed by a 7s pause. In the second cycle, treatment was carried out for 2 s at a voltage of 300 V, followed by cooling in the electrolyte to room temperature. The third sample also underwent cyclic treatment: initial quenching for 2 s at 320 V, followed by a 7s pause. In the second cycle, treatment was carried out for 2 s at a voltage of 300 V, followed by another 7s pause. In the third cycle, treatment was carried out for 2 s at a voltage of 300 V, followed by cooling in the electrolyte to room temperature. The fourth sample underwent quenching for 2 s at a voltage of 320 V, followed by cooling in the electrolyte for 7 s, after which the supply of electrolyte was interrupted.

Table 1. Regimes of 12Kh18N10T steel samples for EPSH.

No.	Regimes	Electrolyte	Voltage (V)	Current (A)	Time (s)
1	Sample No.1	20 wt.% Na_2CO_3 80 wt.% distilled water	320	75	2 s heating–cooling
2	Sample No.2		320 300	80	2 s heating–7 s cooling
3	Sample No.3		320 300 300	80	2 s heating–7 s cooling
4	Sample No.4		320	75	2 s heating–7 s cooling

According to the results of sample tests, the most effective and successful is regime 3. Therefore, regime 3 was chosen for further processing. To ensure uniformity of the hardening process, the part was rotated clockwise during the whole procedural cycle. To reveal the influence of the sample rotation speed on the uniform surface hardening, an experiment was conducted for three applicators with rotation speeds of 4, 6, and 8 rpm. The regimes for the EPSH liquid fertilizer applicator are shown in Table 2.

Table 2. Sample regimes for EPSH needle applicator for liquid fertilizer application.

No.	Regimes	Electrolyte	Voltage (V)	Current (A)	Time (s)	Sample rotation speed, rpm
1	Sample No.1	20 wt.% Na_2CO_3 80 wt.% distilled water	320 300	80	2 s heating–7 s cooling	4
2	Sample No.2		300		2 s heating–7 s cooling	6
3	Sample No.3				2 s heating –7 s cooling	8

X-ray phase analysis was performed on the Xpert PRO PANalytical instrument. During the study, a voltage of 40 kV and a current of 30 mA, Cu-Kα radiation (λ = 1.541 Å) was applied to the anode copper tube in the range from 10 to 90°, the imaging step was 0.02, and the counting time was 0.5 s/step. Phase analysis from the obtained diffractogram lines was performed using the additional software package HighScore Plus and Mach 3. Sample preparation, selection of imaging regimes, and calculation of diffractograms were carried out according to the methods described in [24].

The wear resistance of the surface hardening was determined as the mass loss per unit time in the process of abrasive wear. The tests were carried out on an abrasion test rig using the method described in [25]. The test conditions were as follows: load 44 N, dwell time 10 min, abrasive material–corundum powder with grain size <100 μm.

The friction coefficient was determined on the universal tribometer TRB^3 (Anton Paar, Austria) according to the scheme of friction "ball-on-disk" by sliding the samples without lubrication on the steel plane of the counterbody with a linear speed of 0.05 m/s at room temperature 25 ± 1 °C. The vertical load is 10 N. The counterbody material is $100Cr_6$. The friction coefficient of the tested materials was determined after passing the friction path (L) equal to 100 m [26]. Wear marks and roughness were investigated using a Mitutoyo profilometer model Surftest 410.

Hardness and modulus of elasticity were determined using the FISCHERSCOPE HM2000 S measuring system in accordance with the requirements of DIN EN ISO 14577-1. The test results were processed using WIN-HCU software. The Martens hardness (*HM*) was chosen as a characteristic parameter and calculated according to the following Eq 1 [27]:

$$HM = \frac{F}{A_s\,(h)} \tag{1}$$

where, *HM* is Martens hardness (N/mm^2); *F* is the test load (N); A_s is the indenter cross-sectional area, (mm^2); and *h* is the indenter penetration depth (mm). A load of 1000 mN and a dwell time of 20 s were used during the test to determine the hardness. Ten tests were performed for each sample and the values obtained were averaged to obtain the final value.

The microhardness of the samples was determined on a Metolab 502 instrument according to the Vickers hardness (*HV*) method [18]. The measurement parameters were as follows: load 20 g, dwell time 10 s. Microhardness is calculated by the Eq 2:

$$HV = \frac{1.854P}{d^2} \tag{2}$$

where, *HV* is Vickers hardness (kgf/mm^2); *P* is the applied load (kgf); *d* is the average diagonal of the indenter (mm).

3. Results and discussion

3.1. Investigation of mechanical and tribological properties of 12Kh18N10T steel before and after EPSHE

The method of measuring microhardness and Young's modulus (Figure 1) consists in selecting the parameters of the step function describing the experimental dependence of the indentation depth and contact area on the applied force and calculating the hardness and modulus of elasticity using these data according to [28]. Figure 1 and Table 3 show the results of these studies.

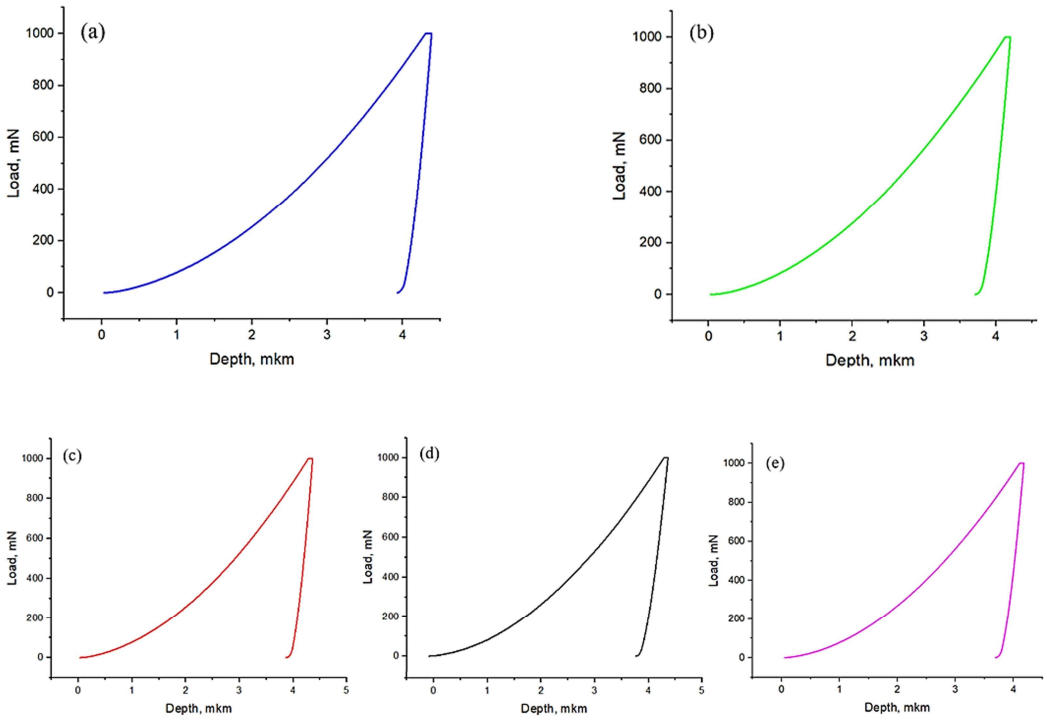

Figure 1. P-h-diagrams–curves of normal force dependence on indenter penetration depth for 12Kh18N10T steel samples: (a) initial sample, (b) No.1, (c) No.2, (d) No.3, (e) No.4–samples after EPSH.

Table 3. Hardness of 2Kh18N10T EPSH steel measured by Fischerscope HM2000 S indentation meter.

Samples	Martens hardness (MPa)	Modulus of elasticity (GPa)	Hardness (HV)
initial	2733.3	198.6	325.6
No. 1	2016.5	174.0	233.4
No. 2	2173.2	182.1	243.0
No. 3	2191.0	185.9	254.8
No. 4	1995.2	189.6	229.1

The higher hardness of the EPSH samples in this experiment significantly limits the deformation depth of the wear surface, which leads to a significant decrease in friction coefficients in accordance with [29]. As can be seen in Figure 2, comparing the friction coefficient values, it can be said that the lower hardness of the sample surface leads to a more pronounced deformation of the material. The relative error of measurements did not exceed 8%.

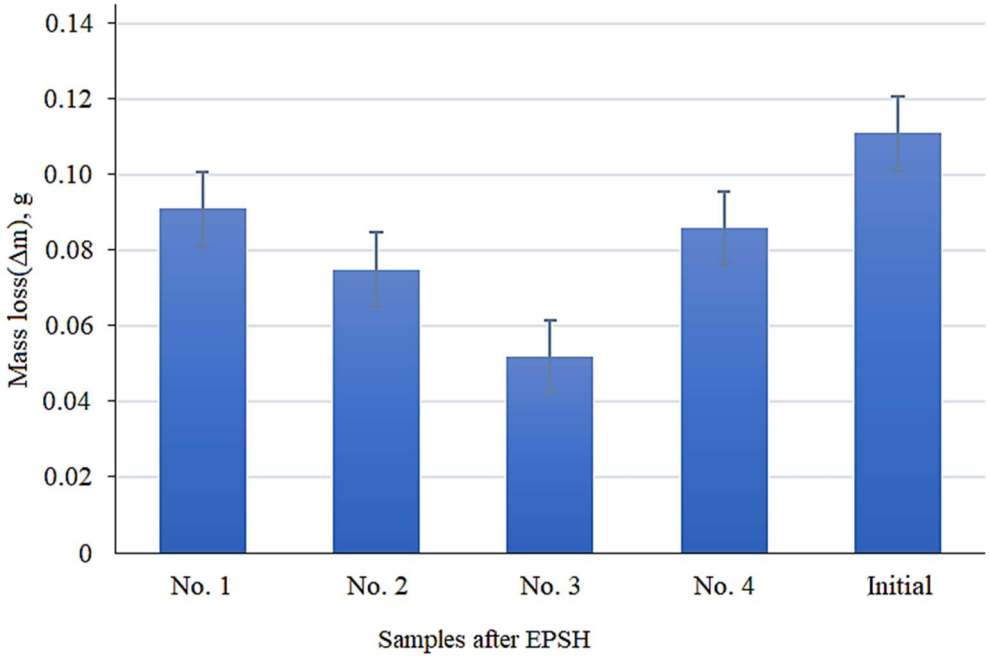

Figure 2. Abrasive wear of 12Kh18N10T steel samples: No. 1, No. 2, No. 3, No. 4– samples after EPSH, end initial sample.

Based on the data obtained, the following regularities can be identified. As can be seen in Figure 3a, the initial structure of the sample of steel 12Kh18N10T is an austenitic (γ) phase. Figure 3b shows the results of X-ray phase analysis of sample No. 3, selected as the hardest sample according to the results of the tests. The X-ray diffractometry analysis showed that after EPSH, the near-surface layer mainly contains austenite (γ-Fe) and ferrite (α-Fe). Austenite has FCC structure, and ferrite has BCC structure. The appearance of new phases can be deduced from the Fe-C state diagram. The presence of austenite phase can be associated with an increase in the temperature of heating for quenching, as there is a complete dissolution of carbide phases and this leads to the stability of residual austenite. According to [30], high cooling rates lead to the formation of ferrite phases in the range of 10%–45% at EPSH.

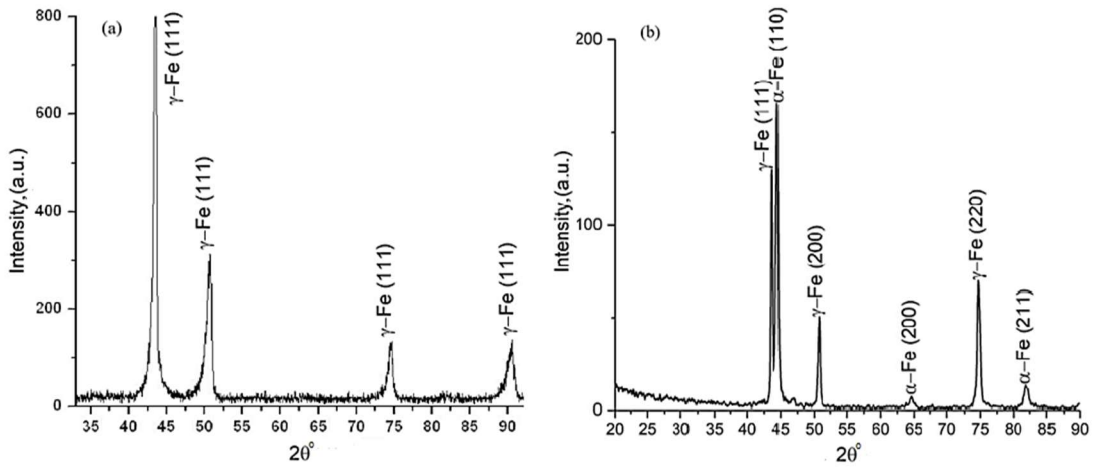

Figure 3. X-ray phase analysis of 12Kh18N10T samples: (a) original sample, (b) sample under regime No.3.

The microstructure of sample No. 3 after EPSH treatment is shown in Figure 4. As can be seen from the optical micrographs, EPSH gives the steel surface the desired aesthetic appearance. This parameter is evaluated by measuring the surface gloss-reflection compared to a reference (mirror, ρ = 100%) and is expressed in percent. After EPSH, the surface gloss increases from 2% to 60%–65% [31].

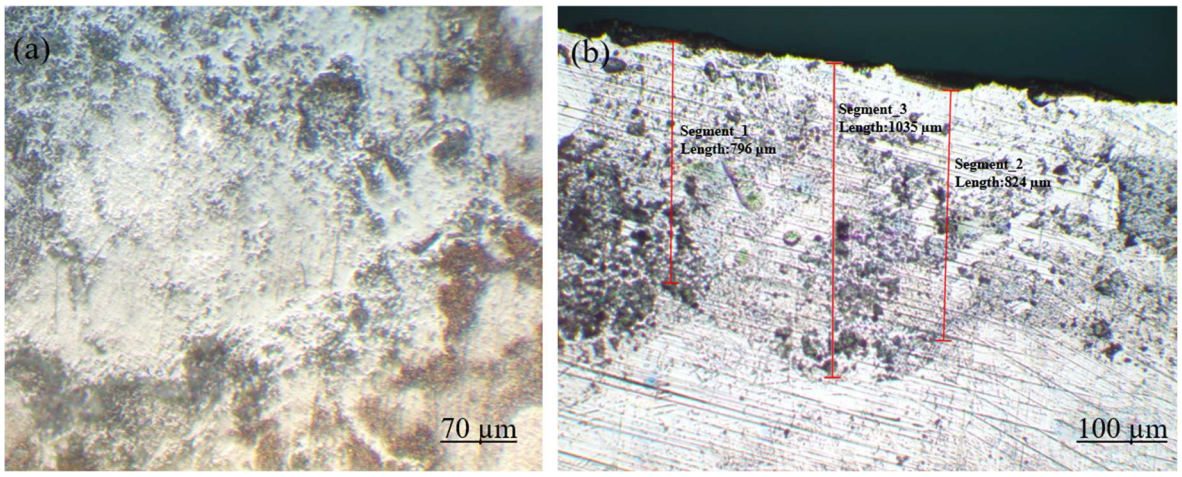

Figure 4. Structure of sample No.3 after EPSH treatment (a) surface, (b) cross section.

Intermittent coupling of the electric potential leads to a periodic increase and stabilizes or slows down the growth of the heating rate, which then allows longer time and a thicker heated layer [29]. The thickness of the layer was measured in cross section using an optical microscope, according to which the average thickness of the coating is 885 µm.

The sliding friction coefficients of the samples under different thermal cycling conditions are shown in Figure 5. The studies show that after EPSH of the sample the coefficient of friction decreases. If the friction coefficient is ~0.8 in the initial state, then it decreases to 0.17 after EPSH. The decrease in the coefficient of friction characterizes the decrease in wear. These data are similar to those obtained in [32], where samples were tested for wear in Ringer's solution. The authors showed that

electrolyte-plasma hardening causes a significant decrease in the coefficient of friction. This index is several times lower than for untreated samples.

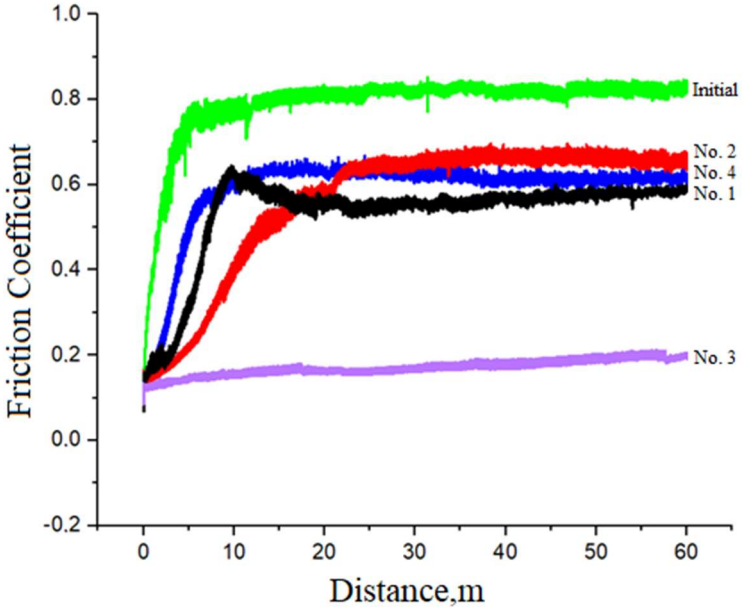

Figure 5. Friction coefficient of 12Kh18N10T steel samples: initial sample end No. 1, No. 2, No. 3, No. 4–samples after EPSH.

3.2. Development of unit for EPSH of steel needles of liquid fertilizer applicator

The specified unit of EPSH is a complex system consisting of two fundamental nodes, each of which performs its specific functions (Figure 6). The first node is represented as a direct current (DC) power supply (Figure 6a), which provides the necessary energy supply for the quenching process. The main component of the power supply is a transformer unit, which has the following characteristics: input voltage 380 V ± 5%, output voltage from the transformer to a maximum of 360 V ± 5%, and power of 40 kW. The transformer is controlled by a thyristor unit consisting of six power thyristors of T142-80-12 brand, which are cooled by radiators of O241 brand. The thyristors work in pairs and each one opens its own arm. The six thyristors are controlled by Arduino Atmega 8 microcontroller through homemade pulse transformers. The pulse transformers are signaled through the ULN2003 chip, which consists of a set of transistors. This node regulates and maintains the specified power supply parameters, which is critical to ensure the stability and efficiency of the quenching process.

Power supply specifications:

- Input: alternating current
- 3 phase voltages: 380~440 V; 50 Hz
- Output: direct (pulsating) current
- Voltage (effective): 100–390 B
- Maximum allowable current: 150 A
- Control: software

The second node is the place where the quenching process of unit applicators is directly carried out (Figure 6b). Its design includes specialized elements and fixtures for fastening and positioning the

work pieces to be processed during heat treatment. This provides optimal conditions for uniform heating and subsequent hardening of each applicator, which in turn contributes to improving the quality and durability of liquid fertilizer units.

Technical characteristics of the quenching unit:

- Input: alternating current
- Voltage: 220~240 V; 50 Hz
- Sample rotation speed 0–9 rpm
- Electrolyte feed rate 0–120 L/min
- Control: software

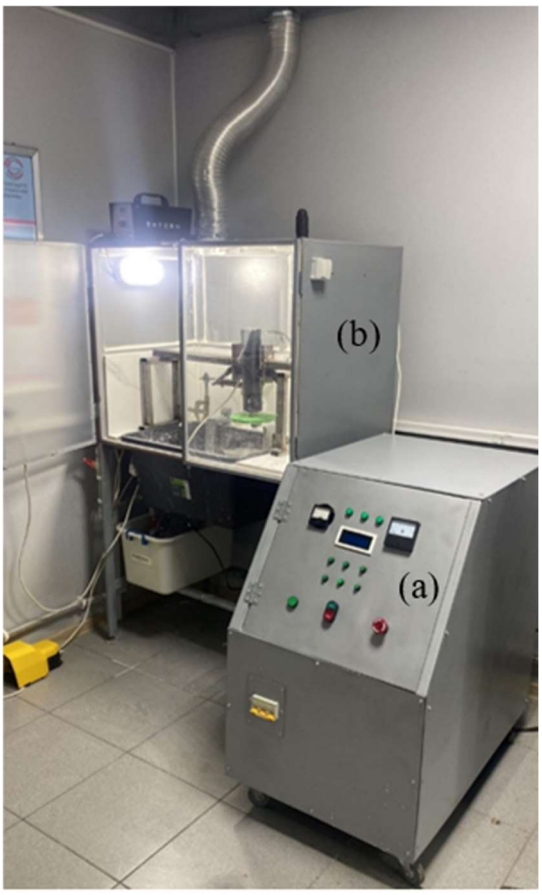

Figure 6. Unit for electrolyte-plasma quenching. (a) Power supply; (b) quench chamber.

For the applicator hardening process, a fixture based on the MINI-15 welding rotator was specially designed and manufactured, in which the applicators are mounted securely and conveniently (see Figure 7). This fixture is designed to provide optimal conditions during quenching operations, which contributes to the quality of the final product. This device allows to ensure correct positioning of the applicator during the quenching process, which in turn guarantees uniform temperature distribution over the entire surface of each applicator, eliminating the risk of deformation or damage to the material. The applicator is mounted in the fixture in such a way as to ensure that they are securely fastened and that they cannot move or fall during the heat treatment process.

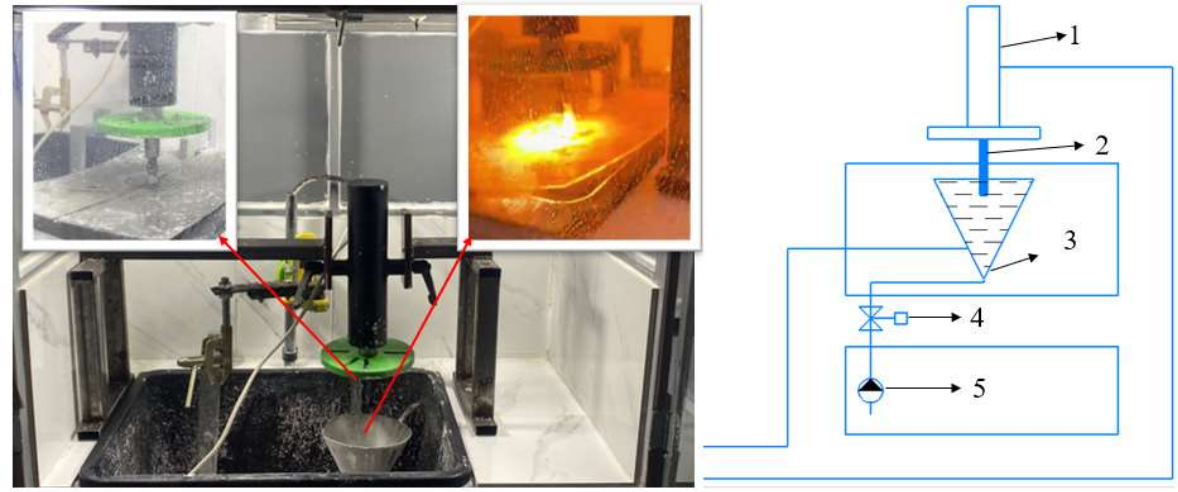

Figure 7. Fixture for fixing the needle (applicators for liquid fertilizer application). 1: sample rotator, 2: applicator, 3: electrolytic cell, 4: regulating valve, 5: pump.

3.3. Investigation of the mechanical properties of steel needles of liquid fertilizer applicator after EPSH

After analyzing the results and comparing them with the characteristics of the needle before treatment, it was concluded that the distribution of microhardness on the surface at 8 rpm was homogeneous and more uniform (Figure 8) and the value of microhardness was about 1.5–2 times higher in HV than the original sample.

The microhardnesses of samples No.1 and No.2 are uneven and in some points of measurement there is a sharp decrease or increase in hardness. In our opinion, this is due to the rotation turnover; the more revolutions, the less irregularities in the distribution of microhardness on the surface of applicators.

On average, the microhardness of the modified surface area reached ~650 HV, with a maximum value of 887.13 HV characteristic of the regime of sample No. 3. The surface microhardness of the initial sample amounted to 392.32 HV.

B. Bordman in his paper [33] presents a table of different hardened steels commonly used for gear manufacturing. He shows, in Rockwell hardness (HRC) units, that the endurance limit of the steel will start to decrease depending on the steel in the range of HRC 40 and above. Therefore, the study of HRC in the range of 20–32 is in agreement with the results of B. Boardman's work.

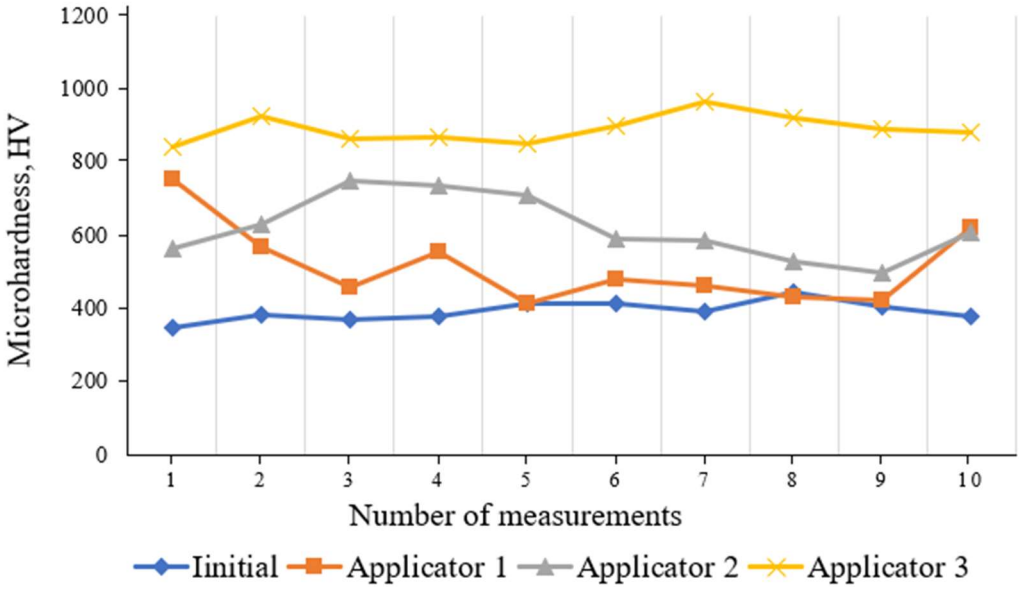

Figure 8. Microhardness of needles of liquid fertilizer applicators, samples by regimes and initial sample.

4. Conclusions

In connection with the above studies of EPSH in different regimes of thermocycling, the optimum regime is that of sample No. 3, which has improved structural-phase and mechanical properties in many parameters. It was found that, as a result of EPSH, the phase composition of the surface of the samples is characterized by the presence of austenite (γ-Fe) and ferrite (α-Fe). Heating of the surface under hardening as a result of EPSH led to stability of residual austenite.

An increase in surface microhardness was observed, with the maximum value reaching 887.13 HV, which corresponds to the regime of sample No. 3. It is revealed that the maximum value of microhardness after EPSH is 2 times higher than the initial value. Also, friction tests revealed that the friction coefficient after EPSH decreased to 0.17, when in the initial state it was ~0.8. This change in friction will contribute to the reduction of wear.

Experiments aimed at the hardening of applicators of aggregates used for liquid fertilizer application were successfully performed on a specialized electrolyte-plasma surface hardening unit designed and manufactured by the team of authors or scientific group of the laboratory. In order to determine the perspectives of the applicators that came out of the research, a contract was made with an agricultural organization for field trials.

Use of AI tools declaration

The authors declare they have not used Artificial Intelligence (AI) tools in the creation of this article.

Funding

This research has been funded by the Science Committee of the Ministry of Science and Higher Education of the Republic of Kazakhstan (Grant No. AP13068365).

Conflict of interest

The authors declare no conflict of interest.

References

1. Nasr GEM, Hamid ZA, Refai M (2023) Agricultural machinery corrosion, In: Singh A, *Introduction to Corrosion-Basics and Advances*, London: IntechOpen. https://doi.org/10.5772/intechopen.108918
2. Sobirjonov A, Alimova ZX, Niyazova GP, et al. (2021) Prevention of corrosion and accelerated wear of agricultural machinery. *IOO-EEO* 20: 7482–7486. https://10.17051/ilkonline.2021.05.848
3. Jain M, Choudhary S, Kumar V (2021) Application of nanotechnology in farm power, machinery and operations: A review. *Agr Eng Today* 45: 1–9. https://10.52151/aet2021454.1541
4. Zabrodin VP (2013) Analysis of factors influencing wear of working surfaces of mineral fertilizer distributors. Mechanization and electrification of animal husbandry, crop production. *Bull Agrar Sci* 4: 44–47 (in Russian).
5. Laguë C, Landry H, Roberge M (2005) Engineering of land application systems for livestock manure: A review. *Can Agric Eng* 47: 17–28.
6. Lyons GA, Cathcart A, Frost JP, et al. (2021) Review of two mechanical separation technologies for the sustainable management of agricultural phosphorus in nutrient-vulnerable zones. *Agronomy* 11: 836. https://doi.org/10.3390/agronomy11050836
7. Yamin M, bin Wan Ismail WI, Abd Aziz S, et al. (2022) Design considerations of variable rate liquid fertilizer applicator for mature oil palm trees. *Precis Agric* 23: 1413–1448. https://doi.org/10.1007/s11119-022-09892-5
8. Thorup-Kristensen K, Kirkegaard J (2016) Root system-based limits to agricultural productivity and efficiency: The farming systems context. *Ann Bot* 118: 573–592. https://doi.org/10.1093/aob/mcw122
9. Zhou W, An T, Wang J, et al. (2023) Design and experiment of a targeted variable fertilization control system for deep application of liquid fertilizer. *Agronomy* 13: 1687. https://doi.org/10.3390/agronomy13071687
10. Liu H (2022) Accelerate the process of intelligent agricultural machinery. *Contemp Farm Mach*.
11. Meikandan M, Karthick M, Natrayan L, et al. (2022) Experimental investigation on tribological behaviour of various processes of anodized coated piston for engine application. *J Nanomater* 2022: 7983390. https://doi.org/10.1155/2022/7983390
12. Maksakova OV, Pogrebnjak AD, Buranich VV, et al. (2021) Theoretical and experimental investigation of multiplayer (TiAlSiY)N/CrN coating before and after gold ions implantation. *High Temp Mater Processes* 25: 57–70. https:// 10.1615/HighTempMatProc.2021038087

13. Dudkina NG, Arisova VN (2021) Surface layer of 40Kh steel after electromechanical treatment with dynamic force impact. *Steel Transl* 51: 235–240. https://doi.org/10.3103/S0967091221040021
14. Rakhadilov B, Bayatanova L, Kurbanbekov S, et al. (2023) Investigation on the effect of technological parameters of electrolyte-plasma cementation method on phase structure and mechanical properties of structural steel 20X. *AIMS Mater Sci* 10: 934–947. https://10.3934/matersci.2023050
15. Yeskermessov D, Rakhadilov B, Zhurerova L, et al. (2023) Surface modification of coatings based on Ni-Cr-Al by pulsed plasma treatment. *AIMS Mater Sci* 10: 755–766. https://10.3934/matersci.2023042
16. Bayati MR, Molaei R, Janghorban K (2011) Surface alloying of carbon steels from electrolytic plasma. *Met Sci Heat Treat* 53: 91–94. https://doi.org/10.1007/s11041-011-9347-5
17. Ayday A, Kırsever D, Demirkıran AS (2022) The effects of overlapping in electrolytic plasma hardening on wear behavior of carbon steel. *Trans Indian Inst Met* 75: 27–33. https://doi.org/10.1007/s12666-021-02368-6
18. Magazov N, Satbaeva Z, Rakhadilov B, et al. (2023) Study on surface hardening and wear resistance of AISI 52100 steel by ultrasonic nanocrystal surface modification and electrolytic plasma surface modification technologies. *Materials* 16: 6824. https://doi.org/10.3390/ma16206824
19. Dayança A, Karaca B, Kumruoglu LC (2017) The cathodic electrolytic plasma hardening of steel and cast iron based automotive camshafts. *Acta Phys Pol A* 131: 374–378. https://10.12693/APhysPolA.131.374
20. Rakhadilov B, Seitkhanova A, Satbayeva Z, et al. (2021) Investigation of the structural, mechanical and tribological properties of plasma electrolytic hardened chromium-nickel steel. *Lubricants* 9: 108. https://doi.org/10.3390/lubricants9110108
21. Kozlov E, Popova N, Zhurerova L, et al. (2016) Structural and phase transformations in 0.3 C-1Cr-1Mn-1Si-Fe steel after electrolytic plasma treatment. *AIP Conf Proc* 1783: 020112. https://doi.org/10.1063/1.4966405
22. Rakhadilov BK, Satbayeva ZA, Bayatanova LB, et al. (2019) Influence of electrolyte-plasma surface hardening on the structure and properties of steel 40KhN. *J Phys Conf Ser* 1393: 012119. https://10.1088/1742-6596/1393/1/012119
23. Rakhadilov B, Baizhan D (2021) Creation of bioceramic coatings on the surface of Ti-6Al-4V alloy by plasma electrolytic oxidation followed by gas detonation spraying. *Coatings* 11: 1433. https://doi.org/10.3390/coatings11121433
24. Skakov M, Bayandinova M, Ocheredko I, et al. (2023) Influence of diabase filler on the structure and tribological properties of coatings based on ultrahigh molecular weight polyethylene. *Polymers* 15: 3465. https:// doi.org/10.3390/polym15163465
25. Rakhadilov BK, Muktanova N, Zhurerova LG (2023) HVOF technology application for wear resistant WC coatings—Review. *NNC RK Bulletin* 1: 4–14 (in Russian). https://doi.org/10.52676/1729-7885-2023-1-4-14
26. Skakov M, Rakhadilov B, Batyrbekov E, et al. (2014) Change of structure and mechanical properties of R6M5 steel surface layer at electrolytic-plasma nitriding. *Adv Mat Res* 1040: 753–758. https://doi.org/10.4028/www.scientific.net/AMR.1040.753

27. Rosentritt M, Hahnel S, Schneider-Feyrer S, et al. (2022) Martens hardness of CAD/CAM resin-based composites. *Appl Sci* 12: 7698. https://doi.org/10.3390/app12157698
28. Baizhan D, Rakhadilov B, Zhurerova L, et al. (2022) Investigation of changes in the structural-phase state and the efficiency of hardening of 30CrMnSiA steel by the method of electrolytic plasma thermocyclic surface treatment. *Coatings* 12: 1696. https://doi.org/10.3390/coatings12111696
29. Sagdoldina Z, Zhurerova L, Tyurin Y, et al. (2022) Modification of the surface of 40 Kh steel by electrolytic plasma hardening. *Metals* 12: 2071. https://doi.org/10.3390/met12122071
30. Proskuryakov VI, Rodionov IV (2022) Development of technology of thin layer laser modification of 12Kh18N10T chromium-nickel steel. *Eng Sci* 3: 85–96 (in Russian). https://doi.org/10.21685/2072-3059-2022-3-9
31. Dai W, Korolev AY, Alekseev YG (2020) Influence of chemical and electrolyte-plasma treatment on the characteristics of working surfaces of ultrasonic waveguides. *Sci Technol Park Poly* 6: 499–506 (in Russian). https://doi.org/10.21122/2227-1031-2020-19-6-499-506
32. Nie X, Tsotsos C, Wilson A, et al. (2001) Characteristics of a plasma electrolytic nitrocarburising treatment for stainless steels. *Surf Coat Technol* 139: 135–142. https://doi.org/10.1016/S0257-8972(01)01025-8
33. Boardman B (1990) Fatigue resistance of steels, In: ASM Handbook Committee, *Properties and Selection, Irons, Steels and High-Performance Alloys*, Kinsman Road: ASM International, 1: 673–688. https://doi.org/10.31399/asm.hb.v01.a0001038

AIMS Press